



Contents lists available at ScienceDirect

## Biochemical and Biophysical Research Communications

journal homepage: [www.elsevier.com/locate/ybbrc](http://www.elsevier.com/locate/ybbrc)

## Structural characterization of *Burkholderia pseudomallei* adenylate kinase (Adk): Profound asymmetry in the crystal structure of the 'open' state

Garry W. Buchko<sup>a,\*</sup>, Howard Robinson<sup>b</sup>, Jan Abendroth<sup>c</sup>, Bart L. Staker<sup>c</sup>, Peter J. Myler<sup>d,e</sup>

<sup>a</sup>Biological Sciences Division and Seattle Structural Genomics Center for Infectious Disease, Pacific Northwest National Laboratory, Richland, WA 99352, USA

<sup>b</sup>Biology Department, Brookhaven National Laboratory, Upton, NY 11973-5000, USA

<sup>c</sup>Emerald Biostructures and Seattle Structural Genomics Center for Infectious Disease, 7869 NE Day Road West, Bainbridge Island, WA 98110, USA

<sup>d</sup>Seattle Biomedical Research Institute and Seattle Structural Genomics Center for Infectious Disease, 307 Westlake Avenue N, Seattle, WA 98109-5219, USA

<sup>e</sup>Department of Medical Education and Biomedical Informatics & Department of Global Health, University of Washington, Seattle, WA 98195, USA

### ARTICLE INFO

#### Article history:

Received 10 March 2010

Available online 21 March 2010

#### Keywords:

Adenylate kinase

Circular dichroism

Conformational transition intermediates

Melioidosis

X-ray crystallography

### ABSTRACT

In all organisms adenylate kinases (Adks) play a vital role in cellular energy metabolism and nucleic acid synthesis. Due to differences in catalytic properties between the Adks found in prokaryotes and in the cytoplasm of eukaryotes, there is interest in targeting this enzyme for new drug therapies against infectious bacterial agents. Here we report the 2.1 Å resolution crystal structure for the 220-residue Adk from *Burkholderia pseudomallei* (BpAdk), the etiological agent responsible for the infectious disease melioidosis. The general structure of apo BpAdk is similar to other Adk structures, composed of a CORE subdomain with peripheral ATP-binding (ATP<sub>bd</sub>) and LID subdomains. The two molecules in the asymmetric unit have significantly different conformations, with a backbone RMSD of 1.46 Å. These two BpAdk conformations may represent 'open' Adk sub-states along the preferential pathway to the 'closed' substrate-bound state.

© 2010 Elsevier Inc. All rights reserved.

### 1. Introduction

Adenylate kinases (Adks) are ubiquitous enzymes in prokaryotes and eukaryotes that catalyze the magnesium-dependent, reversible conversion of ATP and AMP into two molecules of ADP. On the basis of sequence comparisons, they can be organized into two groups composed of short (~190 residues) and long (214–238 residues) variants [1]. Prokaryotes exclusively have the long variant. On the other hand, eukaryotes have both short and long Adk variants that are found in the cytoplasm and the mitochondria, respectively [2]. Several three-dimensional structures of Adks from both variant groups and their subclasses have been determined, with and without bound substrate, and they all share similar tertiary features that may be grouped into three functional subdomains [3]. The core of the protein is composed of a central five-stranded parallel β-sheet surrounded by a number of α-helices (CORE subdomain). On the periphery of the CORE subdomain are the AMP-binding subdomain (AMP<sub>bd</sub>) and the ATP-binding subdomain (LID). The major difference between short and long variant Adks is the size of the LID subdomain due to a 25–40 residue insert

in the long variant. In the catalysis process large conformational changes in the AMP<sub>bd</sub> and LID subdomains occur upon substrate binding with conformational flexibility between open and closed (substrate bound) states intimately linked to catalytic activity [4].

Because Adk proteins play a central role in cellular metabolism and there are significant differences in the catalytic properties between the long variant found in prokaryotes and the short variant found in the cytoplasm of eukaryotes, there is interest in this enzyme as a target for new drugs targeted against infectious bacterial agents. *Burkholderia pseudomallei* is an aerobic, Gram-negative, soil-dwelling bacterium responsible for the infectious disease melioidosis [5]. Melioidosis (aka Whitmore's disease) is a serious health problem in Northern Australia and Southeast Asia, accounting for 40% of all sepsis-related mortality in northeast Thailand. Due to its potential use in biological warfare and biological terrorism, *B. pseudomallei* is also of concern to the U.S. Centers for Disease Control and Prevention. The Adk gene in *B. pseudomallei* codes for a 220-residue protein, BpAdk, that falls into the long variant Adk family. To assist rational structure-based drug design to combat melioidosis and other infectious diseases by exploiting adenylate kinases, the crystal structure for apo BpAdk has been determined to a resolution of 2.1 Å. An unexpected feature of the BpAdk crystal structure was two significantly different conformations of the protein in the asymmetric unit that may represent snapshots of the protein's sub-states.

\* Corresponding author at: Biological Sciences Division, Pacific Northwest National Laboratory, P.O. Box 999, Mail Stop K8-98, Richland, WA 99352, USA. Fax: +1 509 371 6546.

E-mail address: [garry.buchko@pnl.gov](mailto:garry.buchko@pnl.gov) (G.W. Buchko).

## 2. Materials and methods

### 2.1. Cloning, expression, and purification

The *BpAdk* gene (YP\_332492) was amplified using the genomic DNA of *B. pseudomallei* strain 1710b (Q3JK82) and the oligonucleotide primers 5'-GGGTCTCGTTCCGATCGCTTGATCCTGTTGGGCG-3' (forward) and 5'-CTTGTCGTGCTGTTTACTTGTAGCGCGTCGAA-CACGCG-3' (reverse) (Invitrogen, Carlsbad, CA). The amplified *BpAdk* gene was then inserted into the *Nral/Pmel* digested expression vector BG1861 at a site that provided a 8-residue tag (MAH-HHHHH-) at the N-terminal of the expressed protein. The recombinant plasmid was transformed into *Escherichia coli* BL21(DE3) cells (Novagen, Madison, WI) using a heat shock method. Sequencing of the cloned *BpAdk* gene showed a two-nucleotide deletion at position 670 (amino acid position V215), relative to the deposited genome sequence. This small difference at the C-terminus resulted in a clone ending in -RRAQVSE compared to the deposited genome sequence that ends in -FDALK.

Unlabeled and  $^{15}\text{N}$ -labeled *BpAdk* was obtained using a standard minimal media based auto-induction protocol [6] while selenomethionine-substituted *BpAdk* was prepared using a minimal media growth protocol that inhibited the methionine biosynthesis pathway [7]. The latter protocol involved growing the cells at 310 K to mid-log phase ( $\text{OD}_{600\text{nm}} \sim 0.8$ ) in M9 minimal medium supplemented with 100  $\mu\text{g}/\text{mL}$  ampicillin, 120  $\mu\text{g}/\text{mL}$   $\text{MgSO}_4$ , 11  $\mu\text{g}/\text{mL}$   $\text{CaCl}_2$ , 10  $\text{ng}/\text{mL}$   $\text{Fe}_2\text{Cl}_3$ , 50  $\mu\text{g}/\text{mL}$   $\text{NaCl}$ , and 4  $\text{mg}/\text{mL}$  glucose. The temperature was then lowered to 298 K and lysine (0.1  $\mu\text{g}/\text{mL}$ ), phenylalanine (0.1  $\mu\text{g}/\text{mL}$ ), threonine (0.1  $\mu\text{g}/\text{mL}$ ), isoleucine (0.05  $\mu\text{g}/\text{mL}$ ), valine (0.05  $\mu\text{g}/\text{mL}$ ), and selenomethionine (SeMet) (Acros Organics, Geel, Belgium) (0.06  $\mu\text{g}/\text{mL}$ ) were added. Fifteen minutes later protein expression was induced with isopropyl  $\beta$ -D-1-thiogalactopyranoside (0.026  $\text{mg}/\text{mL}$ ). Approximately 6 h later the cells were harvested by mild centrifugation and then frozen at 193 K. Labeled *BpAdk* was purified with a conventional, two-step protocol involving Ni-NTA affinity purification (Qiagen, Valencia, CA) followed by gel-filtration chromatography on a Superdex75 HiLoad 26/60 column (GE Healthcare Life Sciences, Piscataway, NJ) that simultaneously exchanged *BpAdk* into the buffer used for the crystallization and the NMR and CD characterizations (100 mM  $\text{NaCl}$ , 20 mM Tris, 1.0 mM dithiothreitol, pH 7.1).

### 2.2. Nuclear magnetic resonance spectroscopy

The NMR data on the  $^{15}\text{N}$ -labeled *BpAdk* sample (0.5 mM) was collected at 293 K using a Varian Inova-600 spectrometer. An overall rotational correlation time ( $\tau_c$ ) for *BpAdk* was rapidly estimated from backbone amide  $^{15}\text{N}$   $T_{1\rho}/T_1$  ratios [8] measured using a modified  $^1\text{H}$ - $^{15}\text{N}$  HSQC experiment to record an  $^{15}\text{N}$ -edited one-dimensional spectrum.

### 2.3. Circular dichroism spectroscopy

Circular dichroism data for *BpAdk* (4  $\mu\text{M}$ ) were obtained on an Aviv Model 410 spectropolarimeter (Lakewood, NJ). A far-UV wavelength spectrum was recorded between 200 and 260 nm, at 25 °C, in a quartz cell of 0.1 cm path length. The spectrum was the result of averaging two consecutive scans with a step size of 0.5 nm, 1.0 nm bandwidth, and time constant of 1.0 s. The wavelength spectrum was processed by first subtracting a reference spectrum (buffer alone) followed by automated line smoothing. A thermal denaturation curve for *BpAdk* was obtained by recording the ellipticity at 220 nm in 2.0 °C intervals from 10 to 80 °C.

### 2.4. Crystallization

Vapor-diffusion crystallization trials using hanging drops were initially set up on unlabeled *BpAdk* at room temperature ( $\sim 295$  K) using two different protein concentrations ( $\sim 20$  and  $\sim 5$   $\text{mg}/\text{mL}$ ) and screening kits from Hampton Research (Aliso Viejo, CA). Mixing equal volumes of protein and precipitant ( $\sim 1.5$   $\mu\text{L}$ ), crystals appeared 24–48 h later only at the lower protein concentration using precipitant containing 0.2 M  $\text{LiSO}_4$ , 0.1 M  $\text{TrisHCl}$ , 30% (w/v) PEG 4000, pH 8.5. Crystals were cryo-protected by rapid immersion in a drop of the above precipitant containing 15% glycerol, mounted in nylon CryoLoops (Hampton Research), flash-frozen in liquid nitrogen, stored under liquid nitrogen, and shipped to the National Synchrotron Light Source (NSLS) at Brookhaven National Laboratory for X-ray data collection. A similar protocol was used to obtain crystals of SeMet-labeled *BpAdk* with the precipitant conditions identified for the unlabeled protein.

### 2.5. Structure determination and refinement

All X-ray diffraction data (XRD) were collected at the X29A beamline with an ADSC Q315 CCD detector. Data was initially collected on native crystals that diffracted to a resolution of 2.6 Å, however, it was not possible to obtain a molecular replacement solution. A three-wavelength MAD data set at 2.1 Å resolution was collected for a SeMet-*BpAdk* crystal, the peak wavelength data set was sufficient for solving the structure. The data were reduced with the programs XDS and XSCALE [9]. Anomalous signal was assessed with SHELXC and found to extend to the highest resolution shell. Ten selenium sites were determined using SHELXD [10]. The program SHARP [11] was then used for the refinement of the selenium sites and for initial phasing. Phases were improved using density modification and density averaging techniques as implemented in PARROT [12]. Already here the asymmetry between the two NCS copies of *BpAdk* became obvious: maps were clearer when no NCS averaging was used. An initial model was automatically built with BUCCANEER [13], which was then extended with ARP/wARP [14]. The model was then manually inspected in COOT [15] and refined with REFMAC5 (v.5.5.0088) [16]. A final check on the stereochemical quality of the final model was assessed using the program MolProbity [17] and PROCHECK [18] and any conflicts addressed. MolProbity analysis indicated that the overall geometry of the final model ranked in the 95th percentile (MolProbity score of 1.64) where the 100th percentile is best among structures of comparable resolution. The clash score for “all-atoms” was 13.4 corresponding to a 72nd percentile ranking for structures of comparable resolution. PROCHECK analysis showed that 98% of the psi/phi pairs were in most favored region and the remainder in additionally allowed regions. The data collection and structure refinement statistics are given in Table 1 and the coordinates have been submitted to the Protein Data Bank (PDB ID 3GMT).

## 3. Results and discussion

### 3.1. Solution properties of *BpAdk*

The *BpAdk* protein expressed extremely well at  $\sim 150$  and  $\sim 40$   $\text{mg}/\text{L}$  using the auto-induction and SeMet-labeling protocols, respectively. The protein had a retention time on a size exclusion column expected for a monomeric 24.2 kDa protein. The non-associated nature of *BpAdk* in solution was corroborated by the overall rotational correlation time ( $\tau_c$ ) value estimated from NMR experiments,  $15.4 \pm 0.1$  ns at 20 °C. The  $^1\text{H}$ - $^{15}\text{N}$  HSQC spectrum of *BpAdk* showed a wide dispersion of amide chemical shifts in both the proton and nitrogen dimension, features characteristic of a structured

**Table 1**  
Summary of the diffraction data collection and refinement statistics for *BpAdk*.

<i>Data collection</i>	
X-ray source	X29
Detector	ADSC Q315 CCD
X-ray wavelength (Å)	0.9791
Temperature (K)	100
Data set	SAD
Space group	P2 <sub>1</sub>
<i>Unit-cell parameters</i>	
<i>a</i> (Å)	62.23
<i>b</i> (Å)	66.00
<i>c</i> (Å)	63.76
$\alpha = \gamma$	90°
$\beta$	113.69°
Resolution range (Å)	20–2.1 (2.15–2.10) <sup>a</sup>
Mean <i>I</i> / $\sigma$ ( <i>I</i> )	17.0 (3.1) <sup>a</sup>
Completeness (%)	99.5 (99.8) <sup>a</sup>
Redundancy	7.4 (7.6) <sup>a</sup>
<i>R</i> <sub>merge</sub> (%)	7.2 (61.8) <sup>a</sup>
<i>R</i> <sub>means</sub> (%)	7.7 (66.4) <sup>a</sup>
<i>Phasing</i>	
Se sites	10
FOM (Sharp)	0.428
FOM (DM)	0.805
<i>Refinement</i>	
<i>R</i> <sub>work</sub> (%)	23.8
<i>R</i> <sub>free</sub> (%)	29.5
RMSB bonds (Å)	0.015
<i>Model validation</i>	
MolProbity Ramachandran analysis	
Most favored	98%
Additionally allowed	2%
MolProbity	
Clash score, all atoms	13.4 [72th]
MolProbity score	1.64 [95th]

<sup>a</sup> Value in parenthesis are statistics for the highest resolution shell (2.15–2.10 Å).

protein (data not shown). Such a conclusion was supported by the far-UV CD spectrum for *BpAdk*, shown in Fig. 1A. The dominant feature of the CD spectrum is the double minimum at 222 and 208–210 nm and an extrapolated maximum between 190 and 195 nm, features characteristic of a protein with considerable helical secondary structure [19]. The thermal stability of *BpAdk* was assayed by monitoring the ellipticity at 220 nm as a function of

temperature between 10 and 80 °C. As shown in Fig. 1B, a gradual decrease in the ellipticity at 220 nm was observed from 10 to ~38 °C, upon which a steep decrease occurred up to ~45 °C at which point a plateau was reached. The inflection point for the transition was approximately 42 °C. Such a decrease in ellipticity with heating is typical of a phase transition from a folded to denatured state [20]. The process was irreversible with a white precipitant visible in the CD cell after heating. Relative to Adks from *Mycobacterium tuberculosis* and *E. coli*, that had higher melting temperatures of 64.8 and 52.5 °C, respectively, *BpAdk* appeared to be relatively thermally labile [21].

### 3.2. Crystal structure of *BpAdk*

The crystal structure of *BpAdk* was determined at 2.1 Å resolution by single wavelength anomalous scattering. Two molecules were observed in the asymmetric unit of the *BpAdk* crystal and they both exhibited a similar general topology with each other and with other solved Adk structures. As illustrated with the A chain of *BpAdk* in Fig. 2A, the protein is a single  $\alpha\beta$  domain that may be divided into the three functional subdomains highlighted in Fig. 2B. The CORE of the structure (gold) consists of a five-strand, open-twisted, parallel  $\beta$ -sheet ( $\beta_2$ : $\beta_3$ : $\beta_1$ : $\beta_4$ : $\beta_7$ ) sandwiched in between helices  $\alpha_1$  on one face and  $\alpha_5$  and half of  $\alpha_7$  on the other face. Adjacent to the CORE are the AMP<sub>bd</sub> (magenta) and LID (blue) subdomains orientated at an approximate right angle about the CORE subdomain. The AMP<sub>bd</sub> subdomain binds AMP and is composed of three sequential  $\alpha$ -helices,  $\alpha_2$  through  $\alpha_4$ , set in a triangular-like configuration. The LID subdomain contains the ATP-binding site and is composed of a two-strand anti-parallel  $\beta$ -sheet along with  $\alpha_6$  and the other half of  $\alpha_7$ .

Also observed in the crystal structure were two sulfate ions as shown in Fig. 3. One is in the CORE subdomain, ligated to the backbone amides of G10, G12, and K13, residues near the N-terminal end of helix-1. The other is in the LID subdomain, held in place by the terminal atoms of the R119 and R123 side chains on  $\alpha_6$  and  $\beta_5$ , respectively. These interactions are similar to the contacts made by the phosphate groups of ADP bound to *M. tuberculosis* Adk [22] and are residues that are highly conserved in all Adks [2,23]. Hence, it is likely that the sulfate groups observed in *BpAdk* are occupying sites typically occupied by the phosphate groups of the protein's natural substrates.

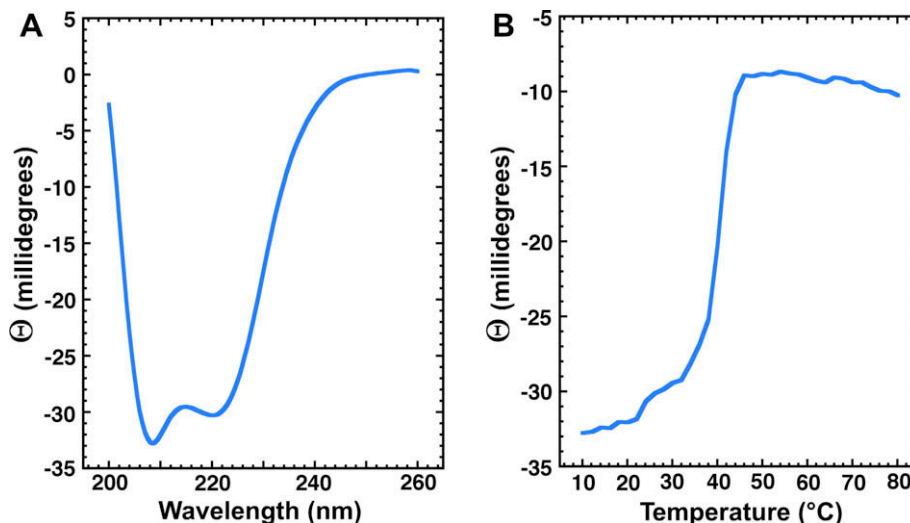


**Fig. 1.** (A) Circular dichroism spectrum of *BpAdk* (4  $\mu$ M) at 25 °C in buffer containing 100 mM NaCl, 20 mM Tris, 1 mM DTT, pH 7.1. (B) CD thermal melt for *BpAdk* (4  $\mu$ M) collected at 220 nm in 2.0 °C intervals between 10 and 80 °C.

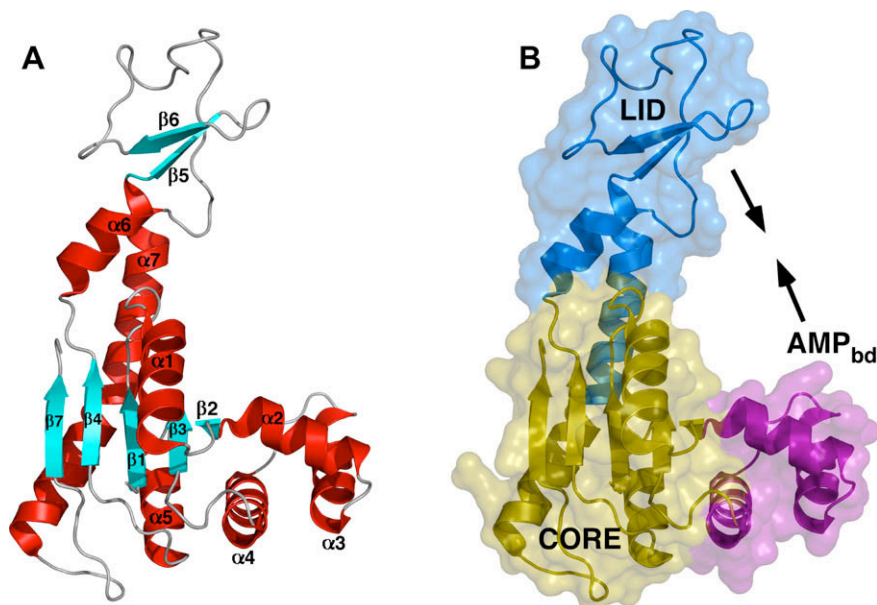


**Fig. 2.** (A) Cartoon representation of one of the two molecules in the asymmetric unit in the crystal structure of *BpAdk* (3GMT-A). Each protein contains seven  $\alpha$ -helices and seven  $\beta$ -strands organized into a five-strand parallel  $\beta$ -sheet and a two-strand anti-parallel  $\beta$ -sheet. Helices are colored red and  $\beta$ -strands cyan. (B) Organization of the protein into the three functional subdomains characteristic of all adenylate kinases: CORE = gold, AMP<sub>bd</sub> = purple (S30–A75), LID = blue (P112–T175). Upon binding substrate the LID and AMP<sub>bd</sub> region swing towards each other as shown by the arrows. (For interpretation of the references to color in this figure legend, the reader is referred to the web version of this article.)

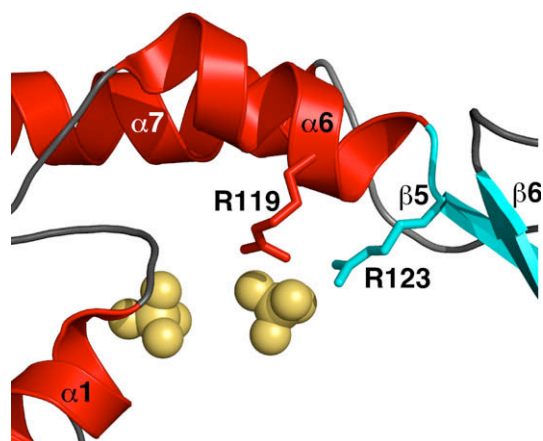


**Fig. 3.** Cartoon representation of the position of the two sulfates ions (spheres) observed in the *BpAdk* crystal structure. One sulfate ion is ligated to the backbone amides of residues G10, G11, and K13. The second sulfate ion is ligated to the terminal ends of the R119 and R123 side chains.

### 3.3. Sub-state snapshots

Despite the significant number of solved adenylate kinases structures in the Protein Data Bank, it was not possible to obtain a molecular replacement solution for X-ray diffraction data collected on native *BpAdk* crystals. To make certain the correct protein had been crystallized, the cloned plasmid used to prepare the protein was sequenced. The first 215 residues of the cloned gene agreed with the deposited sequence for *B. pseudomallei* strain 1710b (Q3JK82). The only difference was that the clone contained the sequence – RRAQVSE following V215 while the expected C-terminus was – FDALK. Regardless of whether the difference was due to an error incurred during cloning or an error in the sequenced genome, such a small change should not effect the success of a molecular replacement search to solve the structure for XRD data

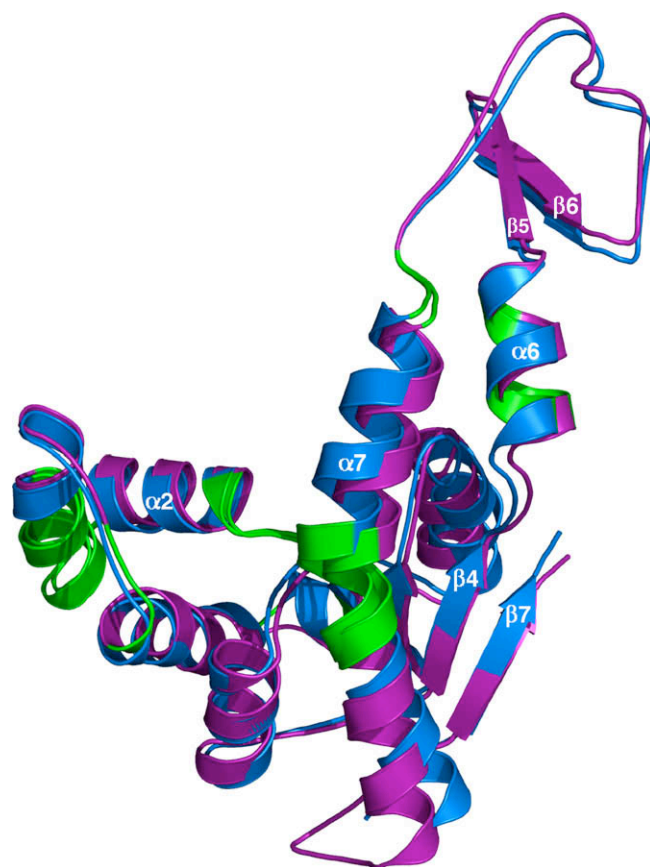


**Fig. 4.** Superposition of the two molecules, A (purple) and B (blue), in the asymmetric unit of apo *BpAdk* using the program SuperPose [33]. The regions in green are the corresponding highly conserved hinge regions identified in *A. aeolicus* Adk [23]. (For interpretation of the references to color in this figure legend, the reader is referred to the web version of this article.)

**Table 2**

Comparison of the RMSD (Å) between molecules in the asymmetric unit of apo adenylate kinase crystal structures.

Organism	PDB ID	Residues	C $\alpha$ (Å)	Backbone (Å)	Heavy (Å)
<i>Burkholderia pseudomallei</i> (all)	3GMT	1–190, 195–203	1.44	1.46	1.60
<i>B. pseudomallei</i> (hinges)	3GMT	29–31, 42–50, 59–61, 74, 79–81, 115–116, 120, 1258–161, 173–177	0.90	0.88	1.26
<i>Escherichia coli</i>	4AKE	1–214	0.61	0.63	0.89
<i>Aquifex aeolicus</i>	2RH5 AB	1–202	1.18	1.19	1.50
<i>Aquifex aeolicus</i>	2RH5 AC	2–202	2.56	2.58	2.72
<i>Aquifex aeolicus</i>	2RH5 BC	1–202	2.09	2.09	2.33

collected on native *BpAdk* crystals unless the structure for *B. pseudomallei* Adk was significantly different from all the other Adk structures. To test the latter hypothesis *BpAdk* was SeMet labeled and the structure solved by MAD phasing. As illustrated in Fig. 4, a superposition of the two *BpAdk* molecules in the asymmetric unit, there is a profound asymmetry in the structure of the two *BpAdk* molecules in the asymmetric unit. The root mean square deviation (RMSD) between all the backbone atoms of each subunit is 1.46 Å and, as listed in Table 2, this is larger than the RMSD between the two subunits in the crystal structure of *E. coli* Adk in the open state. Hence, the reason the native *BpAdk* XRD data could not be solved by molecular replacement methods was not because the *BpAdk* structure differed significantly from other solved adenylate kinase structures, but, because the structure of the two molecules of *BpAdk* in the asymmetric unit differed enough to prevent the acquisition of a molecular replacement solution.

Different conformations of the same protein in the same crystal have been previously observed [24–26], however, the phenomenon is more frequent in crystals with lattice sites occupied by protein in the ligand-free and ligand-bound state(s) [25,27]. One example of a crystal structure containing different conformations of a protein in a ligand-free state is *Aquifex aeolicus* Adk where three distinct ligand-free conformations were observed [25]. As listed in Table 2, the backbone RMSD between the three *A. aeolicus* Adk structures is 1.19, 2.09, and 2.58 Å. Using a multi-pronged suite of NMR, single molecule FRET, normal mode analysis (NMA), and molecular dynamic simulations experiments, a convincing argument was presented that the three conformations observed in the crystal structure of *A. aeolicus* Adk represented snapshots along the preferential reaction pathway towards enzymatic catalysis [25]. In the process of moving from the open to the closed state eight hinge regions were identified in *A. aeolicus* Adk about which movement occurred [23]. The amino acid sequences of these hinge regions are highly conserved among Adks and the corresponding hinge regions are highlighted in green for *BpAdk* in Fig. 4. Collectively, the eight predicted hinge regions in *BpAdk* overlay upon each other better than the protein as a whole with a backbone RMSD of 0.88 Å versus 1.46 Å (Table 2). This suggests that the profound asymmetry observed in the two molecules in the asymmetric unit of *BpAdk* may also represent two snapshots along the pathway towards the closed, enzymatically active state that arise due to movement about the conserved hinge regions.

#### 4. Conclusions

It is well known that LID and AMP<sub>bd</sub> subdomains of adenylate kinases are highly dynamic [25] and undergo significant spatial and dynamic transitions upon binding ATP and AMP [3,28,29]. In the process, the LID and AMP<sub>bd</sub> subdomains swing about conserved hinge regions to fold over the substrates and effect catalysis [23]. For example, the backbone RMSD between the open and closed states of *E. coli* Adk is approximately 7 Å [30,31]. Due, in part, to the large conformational changes between the open and closed states, Adks have served as an excellent model system to study the relationships between enzyme structure, enzyme dynamics,

and enzyme function [25,31,32]. The two conformations of *BpAdk* observed in the crystal structure reported here represent two more structure snapshots to further study the relationships between enzyme structure, dynamics, and function. A better understanding of these relationships for adenylate kinases will assist the rational structure-based design of drugs to combat melioidosis and other infectious diseases.

#### Acknowledgments

This research was funded by NIAID under Federal Contract No. HHSN272200700057C. Major portions of the research was conducted at the W.R. Wiley Environmental Molecular Sciences Laboratory, a national scientific user facility sponsored by U.S. Department of Energy's Office of Biological and Environmental Research (BER) program located at Pacific Northwest National Laboratory (PNNL). PNNL is operated for the U.S. Department of Energy by Battelle. The assistance of the X29A beam line scientists at the National Synchrotron Light Source at Brookhaven National Laboratory is appreciated. Support for beamline X29A at the National Synchrotron Light Source comes principally from the Offices of Biological and Environmental Research and of Basic Energy Sciences of the US Department of Energy, and from the National Center for Research Resources of the National Institutes of Health. The authors thank Dr. Sam Miller (University of Washington) for kindly providing the *B. pseudomallei* strain 1710b (Q3JK82) genomic DNA, Drs. Alberto J. Napuli and Stephen N. Hewitt for preparing the clone, and the support of the SSGCID team.

#### References

- [1] K. Fukami-Kobayashi, M. Nosaka, A. Nakazawa, M. Go, Ancient divergence of long and short isoforms of adenylate kinase: molecular evolution of the nucleoside monophosphate kinase family, *FEBS Lett.* 385 (1996) 214–220.
- [2] H. Yan, M.-D. Tsai, Nucleoside monophosphate kinases: structure, mechanism, and substrate specificity, *Adv. Enzymol. Relat. Areas Mol. Biol.* 73 (1999) 103–134.
- [3] G. Schulz, C.W. Muller, K. Diederichs, Induced-fit movements in adenylate kinases, *J. Mol. Biol.* 213 (1990) 627–630.
- [4] L. Rundqvist, J. Aden, T. Sparrman, M. Wallgren, U. Olsson, M. Wolf-Watz, Noncooperative folding of subdomains in adenylate kinase, *Biochemistry* 48 (2009) 1911–1927.
- [5] W.J. Wiersinga, T. van der Poll, N.J. White, N.P. Day, S.J. Peacock, Melioidosis: insights into the pathogenicity of *Burkholderia pseudomallei*, *Nat. Rev. Microbiol.* 4 (2006) 272–282.
- [6] F.W. Studier, Protein production by auto-induction in high-density shaking cultures, *Protein Expr. Purif.* 41 (2005) 207–234.
- [7] S. Doublet, Preparation of selenomethionyl proteins for phase determination, *Methods Enzymol.* 276 (1997) 523–530.
- [8] T. Szyperki, D.C. Yeh, D.K. Sukumaran, H.N.B. Moseley, G.T. Montelione, Reduced-dimensionality NMR spectroscopy for high-throughput protein resonance assignment, *Proc. Natl. Acad. Sci. USA* 99 (2002) 8009–8014.
- [9] W. Kabsch, Automatic processing of rotation diffraction data from crystals of initially unknown symmetry and cell constants, *J. Appl. Crystallogr.* 26 (1993) 795–800.
- [10] T.R. Schneider, G.M. Sheldrick, Substructure solution with SHELXD, *Acta Crystallogr.* 58 (2002) 1772–1779.
- [11] G. Bricogne, C. Vonrhein, C. Flensburg, M. Schiltz, W. Paciorek, Generation, representation and flow of phase information in structure determination: recent developments in and around *SHARP 2.0*, *Acta Crystallogr. D59* (2003) 2023–2030.
- [12] K.Y. Zhang, K. Cowtan, P. Main, Combining constraints for electron-density modification, *Methods Enzymol.* 277 (1997) 53–64.

- [13] K. Cowtan, The *Buccaneer* software for automated model building. 1. Tracing protein chains, *Acta Crystallogr. D* 62 (2006) 1002–1011.
- [14] A. Perrakis, R. Morris, V.S. Lamzin, Automated protein model building combined with iterative structure refinement, *Nat. Struct. Biol.* 6 (1999) 458–463.
- [15] P. Emsley, K. Cowtan, Coot: model-building tools for molecular graphics, *Acta Crystallogr. D* 60 (2004) 2126–2132.
- [16] G.N. Murshudov, A.A. Vagin, E.J. Dodson, Refinement of macromolecular structures by the maximum-likelihood method, *Acta Crystallogr. D* 53 (1997) 240–255.
- [17] S.C. Lovell, I.W. Davis, W.B. Arendall III, P.I.W. de Bakker, J.M. Word, M.G. Prisant, J.S. Richardson, D.C. Richardson, Structure validation by  $C\alpha$  geometry:  $\pi$ ,  $\sigma$ , and  $C\beta$  deviation, *Proteins* 50 (2003) 437–450.
- [18] R.A. Laskowski, J.D. Watson, J.M. Thornton, From protein structure to biochemical function?, *J. Struct. Funct. Gen.* 4 (2003) 167–177.
- [19] R.W. Woody, Circular dichroism, *Methods Enzymol.* 246 (1995) 34–71.
- [20] G.W. Buchko, N.J. Hess, V. Bandaru, S.S. Wallace, M.A. Kennedy, Spectroscopic studies of zinc(II)- and cobalt(II)-associated *Escherichia coli* formamidopyrimidine-DNA glycosylase (Fpg): extended X-ray absorption fine structure evidence for a metal-binding domain, *Biochemistry* 40 (2000) 12441–12449.
- [21] H. Munier-Lehmann, S. Burlacu-Miron, C.T. Craescu, H.H. Mantsch, C.P. Schultz, A new subfamily of short bacterial adenylate kinases with the *Mycobacterium tuberculosis* enzyme as a model: a predictive and experimental study, *Proteins* 36 (1999) 238–248.
- [22] M. Bellinzoni, A. Haouz, M. Grana, H. Munier-Lehmann, W. Shepard, P.M. Alzari, The crystal structure of *Mycobacterium tuberculosis* adenylate kinase in complex with two molecules of ADP and  $Mg^{2+}$  supports an associative mechanism for phosphoryl transfer, *Protein Sci.* 15 (2006) 1489–1493.
- [23] K.A. Henzler-Wildman, M. Lei, V. Thai, J. Kerns, M. Karplus, D. Kern, A hierarchy of timescales in protein dynamics is linked to enzyme catalysis, *Nature* 450 (2007) 913–916.
- [24] H.R. Raber, B.W. Matthews, A mutant T4 lysozyme displays 5 different crystal conformations, *Nature* 348 (1990) 263–266.
- [25] K.A. Henzler-Wildman, V. Thai, M. Lei, M. Ott, M. Wolf-Watz, T. Fenn, E. Pozharski, M.A. Wilson, G.A. Petsko, M. Karplus, C.G. Hubner, D. Kern, Intrinsic motions along an enzymatic reaction trajectory, *Nature* 450 (2007) 838–844.
- [26] D.T. Gallagher, N. Smith, S.-K. Kim, H. Robinson, P.T. Reddy, Profound asymmetry in the structure of the cAMP-free cAMP receptor protein (CRP) from *Mycobacterium tuberculosis*, *J. Biol. Chem.* 284 (2009) 8228–8232.
- [27] M. Hogg, S.S. Wallace, S. Double, Crystallographic snapshots of a replication DNA polymerase encountering an abasic site, *EMBO J.* 23 (2004) 1483–1493.
- [28] C. Vornrhein, G.J. Schlauederer, M. Schiltz, Movie of the structural changes during a catalytic cycle of nucleoside monophosphate kinases, *Structure* 3 (1995) 483–490.
- [29] Y.E. Shapiro, M.A. Sinev, E.V. Sineva, V. Tugarinov, E. Meirovitch, Backbone dynamics of *Escherichia coli* adenylate kinase at the extreme stages of the catalytic cycle studied by  $(15)N$  NMR relaxation, *Biochemistry* 39 (2000) 6634–6644.
- [30] C.W. Muller, G.J. Schlauederer, J. Reinstein, G.E. Schulz, Adenylate kinase motions during catalysis: an energetic counterweight balancing substrate binding, *Structure* 4 (1996) 147–156.
- [31] O. Beckstein, E.J. Denning, J.R. Perilla, T.B. Woolf, Zipping and unzipping of adenylate kinase: atomistic insights into the ensemble of open closed transitions, *J. Mol. Biol.* 394 (2009) 160–176.
- [32] J. Aden, M. Wolf-Watz, NMR identification of transient complexes critical to adenylate kinase catalysis, *J. Am. Chem. Soc.* 129 (2007) 14003–14012.
- [33] R. Maiti, G.H. Van Domselaar, H. Zhang, D.S. Wishart, SuperPose: a simple server for sophisticated structural superposition, *Nucleic Acids Res.* 23 (2004) W590–W594.